

A simple argument that small hydrogen may exist

J. Va'vra

SLAC, Menlo Park, CA 94025-701, U.S.A.
e-mail: jjv@slac.stanford.edu

Abstract – This paper examines the possible existence of a tightly bound electron–proton state (“small hydrogen”) with a characteristic radius of a few femtometers. Motivated by earlier suggestions of deep relativistic solutions in the Dirac equation, we develop an approximate stability model based on the relativistic virial theorem, incorporating finite-size nuclear potentials, relativistic kinetic energy, and spin–magnetic and spin–orbit corrections. This approach yields a self-consistent estimate of the state’s radius, central binding energy, and hyperfine structure. The predicted signatures—a central binding-energy scale near ≈ 256 keV and a hyperfine transition near 100 ± 30 keV—provide specific experimental targets. If such compact e–p states form efficiently, they could have implications for astrophysics, fusion concepts, and dark-matter phenomenology.

Key words: small hydrogen; relativistic bound states; virial theorem; femtometer-scale atoms

Introduction

In 1920, Rutherford suggested that an electron and proton could be bound in a compact state [1], and tasked Chadwick with searching for it. Following the 1932 discovery of the neutron, the possibility that it represented such an e–p bound system was seriously considered [2]. Heisenberg, among others, initially supported this interpretation before Pauli’s spin–statistics arguments established the neutron as an elementary fermion. This historical discussion is not the focus here, but it illustrates that tightly bound e–p states have been considered since the early development of quantum theory.

Schrödinger, Dirac, and Heisenberg likely recognized formal compact solutions in the Dirac equation, but because the corresponding wavefunctions diverged for a point-like proton, these were discarded [3]. Thus, the concept of “small hydrogen” was set aside for decades.

The idea was later revived by Maly and Va'vra [4,5], who noted that at radii comparable to the proton charge distribution, the electron experiences a non-Coulomb effective potential such as the Smith–Johnson [6] or Nix [7] form, used in relativistic Hartree–Fock treatments of heavy atoms. These authors retained the deep branch of Dirac solutions (the so-called Deep Dirac Levels, DDL). However, it was subsequently realized that the original potential models did not satisfy the relativistic virial balance required for stability.

Brodsky argued that the Dirac equation in single-particle form is inadequate at these distances, and instead advocated a two-body QED treatment (Salpeter–Bethe formalism) [8]. Spence and Vary applied such QED methods and found indications of a deep bound state [9],

but did not pursue the solution further due to its computational complexity.

The difficulty is twofold: (a) the lack of an experimentally confirmed signature, and (b) the theoretical challenge of describing a strongly relativistic two-body bound system at femtometer scales, where wavefunction regularization and higher-order QED effects are essential. In this work, we do not attempt a full QED solution. Instead, we employ an approximate approach based on:

1. the relativistic virial stability condition,
2. the de Broglie wavelength constraint for a circulating relativistic electron,
3. and the requirement of negative total binding energy.

This method provides a physically constrained estimate of the characteristic radius and binding energy.

A tightly bound e–p state cannot form spontaneously from the Coulomb potential alone, because the electron can extract at most ≈ 0.508 MeV from the proton’s static field at $r \approx 2.83$ fm. Formation therefore requires an **external energy input**, analogous to electron capture ($p + e^- \rightarrow n + v_e$), which requires >0.708 MeV.

In the following sections, we analyze the conditions for a stable compact e–p state using the relativistic virial theorem and evaluate the resulting binding energy and hyperfine structure. The role of the Dirac spectrum is discussed only as historical background motivating the existence of deep relativistic solutions; we do **not** rely on the Dirac equation to assert the existence of small hydrogen.

1. Dirac equation effort

Reference [5] applied the Dirac equation to explore whether tightly bound electron–proton states could exist. The Dirac spectrum for a Coulomb potential contains two mathematical branches,

$$s = s(\pm) = \pm ((j + 1/2)^2 - \alpha^2)^{1/2}, \quad (1)$$

with total energy levels according to Sommerfeld-Dirac:

$$E = mc^2 \left(1 + \frac{\alpha^2}{(s+n_r)^2}\right)^{-1/2}, \quad (2)$$

where $j = \ell + \text{spin}$, $\text{spin} = \pm 1/2$, $\ell = k - 1$, $\alpha = e^2/\hbar c = 1/137$, $n_r = 0, 1, 2, 3, \dots$, and $k = 1, 2, 3, \dots$ [11, 12, 13].

The positive branch $s(+)$ reproduces the familiar hydrogen spectrum, while the negative branch $s(-)$ yields extremely deep levels near -509 keV, corresponding to

orbits of a few femtometers. These are the “**Deep Dirac Levels**” (**DDL**) introduced in Refs. [4,5].

Table 1 summarizes these *formal* solutions obtained from Eq. (2). The table is shown here **only** to illustrate the origin of the DDL branch within the Dirac spectrum; the subsequent analysis in this paper does **not** rely on Eq. (2) for quantitative predictions.

Table 1 – Energy levels according to equation (2):

n	k	ℓ	spin	j	Label	E s(+) [eV]	E_{DDL} s(-) [eV]
1	1	0	+1/2	1/2	1s1/2	-13.60589	-13.60587
2	2	1	+1/2	3/2	2p3/2	-3.401435	-3.401435
2	2	1	1/2	3/2	2p3/2	-3.40148	-509134.577
3	2	0	+1/2	3/2	3p3/2	-3.4014358	-3.4014358
3	2	1	-1/2	1/2	3p1/2	-3.301481	-509134.577
3	3	2	1/2	5/2	3d5/2	-1.5117645	-1.5117645
4	4	3	-1/2	5/2	4e5/2	-0.3779367	-510377.569

Note: Label represent a usual spectroscopic notation.

In reality, the proton is not pointlike: its finite charge radius and magnetization profile require replacing the Coulomb potential with a finite-size nuclear potential (e.g., Smith–Johnson or Nix [6,7]). With such potentials, the divergence of the s(-) wavefunction at $r=0$ is regularized, but obtaining fully normalizable solutions requires solving the **two-body** relativistic bound-state problem.

Attempts in our work to obtain compact-state wavefunctions directly from the single-particle Dirac equation with finite-size potentials have not, in our work, yielded stable, square-integrable states. This outcome is consistent with the general viewpoint emphasized by Brodsky and collaborators—that relativistic two-body bound states, especially at short distances, require a full quantum-field-theoretic treatment (light-front QED/QCD) rather than a single-particle Dirac equation [10]. The correct description is a **two-body QED bound-state equation**, such as the Bethe–Salpeter (Salpeter–Bethe) formulation [8].

Spence and Vary [9] implemented such a QED two-body approach and found indications of a deeply bound solution. However, their calculation treated the proton as a pointlike Dirac particle. Extending this method to include the proton’s internal quark structure (QCD) requires solving the coupled problem: $e^- + (uud)_{QCD} \rightarrow$ bound state with photon and gluon exchange. Such a full QED+QCD bound-state calculation has **not** yet been carried out.

Because a complete two-body field-theoretic solution is presently beyond tractable computation, we proceed using a different method. The remainder of this paper employs a relativistic virial-theorem approach, which incorporates:

- relativistic kinetic energy,
- finite-size nuclear potentials,
- and stability (negative total energy) conditions.

2. Simple argument for small hydrogen

We model the system using the relativistic virial theorem, which balances the electron’s relativistic kinetic energy against the attractive and repulsive components of the interaction potential. Because the electron in such a compact configuration is highly relativistic ($\gamma_e \gtrsim 100$), the

stability condition cannot be analyzed using nonrelativistic hydrogenic expressions.

We write the effective interaction energy as the sum of three dominant contributions:

$$U = V_{eff} + V_{(Spin.B)} + V_{SO}$$

Each term is evaluated down to radii $r \sim 1-5$ fm region, a regime in which relativistic, finite-size, and spin effects are significant.

2.1 Effective Coulomb potential V_{eff}

As shown in chapter 4.1, the pure Coulomb potential $V_C = -KZe^2/r$ does not stabilize a relativistic electron at femtometer radii. Following Adamenko & Vysotskii [14], we use the **semi-relativistic effective potential**:

$$V_{eff} = \gamma_e V_c - V_c^2/2m_e c^2, \quad V_c = Ke^2/r \quad (3)$$

which reflects the relativistic balance between the electron’s kinetic momentum and the electromagnetic field energy in a static central potential (here $K = 1/(4\pi\epsilon_0)$).

This expression is **not** a Dirac eigenvalue formula, but an **energy–momentum balance relation** appropriate when the electron is highly relativistic ($\gamma \gg 1$). The second term deepens the potential at small r , making V_{eff} significantly stronger than V_C between ~ 1 and ~ 5 fm (see Fig. 1).

Paillet and Meulenberg [15] independently introduced the same effective potential in the context of compact e–p bound states.

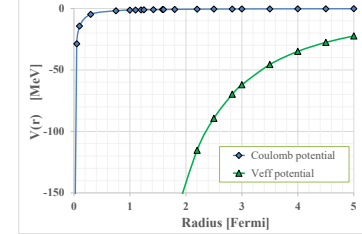


Figure 1 $V_C(r)$ and $V_{eff}(r)$ potential vs. radius.

2.2 Spin-Magnetic Interaction $V_{(Spin.B)}$

At radii $r \sim 2-4$ fm, the proton’s magnetic field is well approximated by its leading dipole term. Finite-size structure effects modify the dipole field only at the few-percent level at these radii; such corrections remain small compared to other theoretical uncertainties in our simplified model. We therefore use the leading dipole form for $B(r)$, which is sufficient for order-of-magnitude estimates of the hyperfine splitting.

The interaction of the electron spin with this magnetic field is

$$V_{(Spin.B)}(r) = -\mu_e B_p(r) = -(g_e \mu_B / \gamma_e) (\boldsymbol{\sigma} \cdot \mathbf{B}_p) \quad (4)$$

where $\mu_e \sim \mu_B / \gamma_e$, $\mu_B = e\hbar/2m_e$, $g_e = 2.00232$ (electron g-factor), $\mu_B = 5.788 \times 10^{-9}$ eV/Gauss (Bohr magneton), the factor $1/\gamma_e$ accounts for the relativistic reduction of the electron’s magnetic moment in the lab/proton rest frame, and the proton magnetic field $B_p(r)$ is modeled as a dipole:

$$B_p(r) \sim (\mu_0 / 4\pi) 2\mu_p / r^3 \quad (5)$$

where $\mu_p = 2.793\mu_N$, $\mu_N = e\hbar/2m_p = 3.152 \times 10 - 8$ eV/T. Evaluating at the virial radius $r = 2.83475$ fm, $B_p \equiv B_{dipole} = 1.238 \times 10^{11}$ T, giving an interaction energy $V_{(Spin.B_p)} \sim -52.6$ keV.

A flip of the electron spin reverses the sign of this term, giving a **hyperfine splitting** $\Delta E_{hf} \sim 2 |V_{(Spin.B)}(r)| \sim 105$ keV. Allowing 10-30% uncertainty from form-factor and tensor-spin corrections, we quote $\sim 100 \pm 30$ keV.

For comparison, ordinary hydrogen has a hyperfine splitting of 5.879×10^{-6} eV (the 21 cm line). The predicted ~ 100 keV transition is therefore a distinct and **experimentally testable signature** of the small-hydrogen model.

2.3 Spin-Orbit interaction V_{SO} (order of magnitude)

For a central **vector** potential $V_C(r)$, the Pauli (Foldy-Wouthuysen) reduction of the Dirac equation yields the standard spin-orbit term [16]

$$V_{SO}(r) = \frac{1}{2m^2c^2} \frac{1}{r} \frac{dV_C}{dr} \quad (6)$$

where the familiar “Thomas factor” 1/2 is already included by virtue of starting from Dirac theory. For a Coulomb potential, where $V_C(r) = -Ze^2/(4\pi\epsilon_0 r)$, $dV_C(r)/dr = Ze^2/(4\pi\epsilon_0 r^2)$, yielding (The Thomas precession factor of 1/2 is already contained in Eq. (6) because it results directly from starting with the Dirac Hamiltonian.):

$$\frac{1}{r} \frac{dV_C}{dr} = \frac{Ze^2}{4\pi\epsilon_0 r^3} \Rightarrow V_{SO}(r) = \frac{Ze^2}{8\pi\epsilon_0 m_e c^2} \frac{(\mathbf{L} \cdot \mathbf{S})}{r^3} \quad (7)$$

In the “small-hydrogen” the electron is highly relativistic ($\gamma_e \sim 100-150$). A full derivation at these fields would require a two-body QED calculation with finite-size proton structure. As a practical approximation, we **scale** the electron mass to its relativistic value $m_e \rightarrow \gamma_e m_e$, giving

$$V_{SO} \sim \frac{Ze^2}{8\pi\epsilon_0 (\gamma_e m_e)^2 c^2} \frac{(\mathbf{L} \cdot \mathbf{S})}{r^3} \quad (8)$$

Thus $V_{SO} \sim 1/\gamma_e^2$ and is strongly suppressed as $\gamma_e \gg 1$. With $\gamma_e \sim 100-150$, V_{SO} is two orders of magnitude smaller than the spin-magnetic $V_{(Spin.B)}$, and three orders of magnitude smaller than dominant binding potential V_{eff} .

The expected sign depends on angular momentum coupling:

- a) $\ell=1, s=1/2, j=3/2$: $(\mathbf{L} \cdot \mathbf{S})/\hbar^2 = 1/2, V_{SO} > 0$,
- b) $\ell=0$: $(\mathbf{L} \cdot \mathbf{S})/\hbar^2 = 0, V_{SO} = 0$,
- c) $\ell=1, s=-1/2, j=1/2$: $(\mathbf{L} \cdot \mathbf{S})/\hbar^2 = -1, V_{SO} < 0$.

As shown in Fig. 2, $|V_{eff}| \gg |V_{(Spin.B)}| \gg |V_{SO}|$. The binding energy and mean radius are therefore determined almost entirely by the virial balance between $T_{kinetic}$ and V_{eff} , while $V_{(Spin.B)}$ sets the dominant observable splitting ~ 100 keV. The spin-orbit term contributes only a much smaller fine-structure correction.

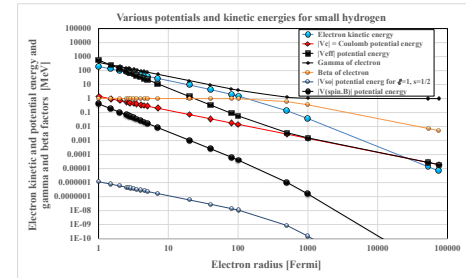


Figure 2 Comparison of electron kinetic energy $T_{kinetic}$, and absolute values of potentials $|V_C|$, $|V_{(Spin.B)}|$, $|V_{SO}|$ (for $\ell=1, s=1/2$), and $|V_{eff}|$; $|V_{eff}| \gg |V_{(Spin.B)}| \gg |V_{SO}|$.

3. Virial theorem stability condition

The virial theorem provides a direct criterion for the stability of a bound two-body system. For a periodic orbit in a central potential $U(r)$, the time-averaged kinetic and potential energies satisfy a definite relation. Although the virial theorem is exact only in the time-averaged sense, the equilibrium radius of a stable bound configuration corresponds to a stationary point of the effective Hamiltonian. In practice, this stable radius is determined by solving the condition (see Appendix #1 for derivation)

$$T_{kinetic}(r_{stable}) = T_{virial}(r_{stable}).$$

This procedure does **not** assume that the electron literally follows a circular orbit. Rather, the circular-orbit configuration is used as a convenient representation of the virial balance point, which is valid for any bound periodic motion (including elliptical or vibrational trajectories) because the virial relations depend only on time-averaged quantities. We determine r_{stable} by iteratively solving the above equality.

Even if the virial equilibrium condition is satisfied, a physically bound state further requires that a negative **total energy**

$$E_{tot}(r) = T_{kinetic}(r) + U(r) < 0,$$

otherwise the configuration corresponds to an unbound scattering state. Thus, the virial condition $T_{kinetic}(r_{stable}) = T_{virial}(r_{stable})$ must always be accompanied by the binding requirement $E_{tot}(r_{stable}) < 0$.

3.1 Electron kinetic energy

For a circular orbit with de Broglie wavelength $\lambda = (2\pi/r)$, the electron momentum is $p(r) = h/\lambda = \hbar n/r$. The corresponding relativistic kinetic energy is

$$\begin{aligned} T_{kinetic} &= \sqrt{(p(r)c)^2 + (m_e c^2)^2} - m_e c^2 \\ &= \sqrt{(hc/\lambda)^2 + (m_e c^2)^2} - m_e c^2 \end{aligned} \quad (10)$$

For small-hydrogen states with $\gamma_e \gg 1$, this can be written equivalently as $T_{kinetic}(r) = (\gamma_e - 1) m_e c^2$.

3.2 Virial kinetic energy

For a general central potential $U(r) = \sum U_i(r)$, where each term behaves locally as $U_i(r) \propto r^{k_i}$ near the candidate radius, the relativistic virial relation gives [16–19]:

$$T_{virial}(r) = \sum k_i [\gamma_e / (\gamma_e + 1)] U_i(r) \quad (11)$$

with $\gamma_e = 1/\sqrt{1 - (v/c)^2}$ the Lorentz factor of electron

Examples:

- For a Coulomb term $U_1 = V_C = -KZe^2/r$, the exponent $k = -1$, so $T_{virial} \rightarrow -(1/2)V_C$ as $\gamma_e \rightarrow 1$, and $T_{virial} \rightarrow -V_C$ for $\gamma_e \rightarrow \infty$.
- For a term $U(r) = 1/r^2$, $k = -2$, giving $T_{virial} \rightarrow -2U$ as $\gamma_e \rightarrow \infty$.
- For present model $U(r) = V_{eff}(r) + V_{(Spin.B)}(r) + V_{SO}(r)$, so:

$$T_{virial} = \frac{\gamma^2}{\gamma+1} |V_C| + 2 \frac{\gamma}{\gamma+1} \frac{V_c^2}{(2m_e c^2)} + 3 \frac{\gamma}{\gamma+1} |V_{(Spin.B)}| - 3 \frac{\gamma}{\gamma+1} V_{SO} \quad (12)$$

(The factor 3 reflects the $1/r^3$ dependence of the magnetic-dipole and spin-orbit terms).

3.3 Virial-equilibrium method

The stable radius is obtained iteratively from:

$$T_{kinetic}(r_{stable}) = T_{virial}(r_{stable}), \quad (13)$$

Which we refer to as **Method A** (direct virial equilibrium)

Figure 3 verifies this condition for ordinary hydrogen, modeled via the Bohr approach; $T_{kinetic}$ uses Eq.(10) and T_{virial} uses Eq.(12). This agrees with the Schrödinger solution, where the virial relation follows expectation values of $\langle V \rangle$ and $\langle r \rangle$.

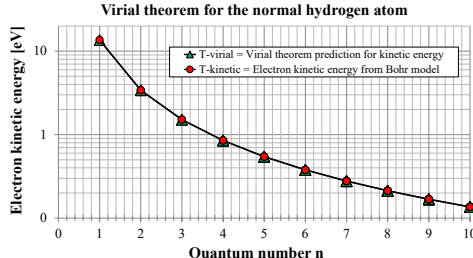


Figure 3 This plot validates equation (11) for the normal hydrogen. Here $T_{kinetic}$ is calculated using equation (10) and T_{virial} is calculated using equation (12).

3.4 Relativistic virial cross-check (Method B)

An equivalent formulation [17] uses

$$\langle \mathbf{p} \cdot \partial/\partial \mathbf{p} T_{kinetic}(p) - \mathbf{r} \cdot \partial/\partial \mathbf{r} U(r) \rangle = 0 \quad (14)$$

For a circular relativistic orbit, this becomes the instantaneous condition (see Appendix #1)

$$((\mathbf{p}c)^2/\sqrt{((\mathbf{p}c)^2 + (m_e c^2)^2)} - \mathbf{r} \cdot \partial/\partial \mathbf{r} (U)) = 0, \quad (15)$$

where $\mathbf{p} = \gamma_e m_e$ and $U = V_{eff} + V_{(Spin.B)} + V_{SO}$. Solving Eq. (15) reproduces the same r_{stable} found from Eq. (13), confirming internal consistency.

This approach is not a first-principles derivation but a constrained energetic model.

4. Results:

4.1 Coulomb potential V_C

Applying the virial-stability method to the pure Coulomb potential

$$V_C = -Ke^2/r,$$

one finds that the Coulomb force alone does not provide a stable small-hydrogen orbit.

Figure 4 shows that the virial condition $T_{kinetic} = T_{virial}$ yields only a single region of stability corresponding to **ordinary hydrogen**, while no equilibrium solution appears for $r < 10$ fm.

Finite-size-corrected Coulomb potentials, such as the Smith-Johnson and Nix forms [4, 5], slightly modify the short-range curvature but still fail to produce a second virial equilibrium point corresponding to a compact small-hydrogen state.

The virial analysis therefore demonstrates that an additional **short-range attractive term** is required to balance the strong relativistic kinetic energy and stabilize an ultra-tight orbit.

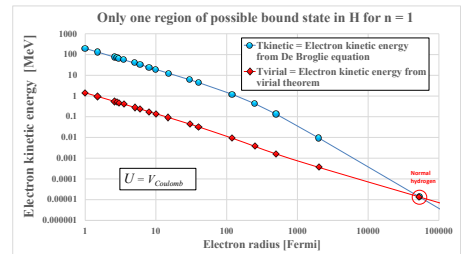


Figure 4 Virial equilibrium for the pure Coulomb potential in the e-p system. Only one stable region appears—corresponding to normal hydrogen. The Coulomb force alone cannot stabilize a deep small-hydrogen orbit.

4.2 Effective potential V_{eff}

Introducing the semi-relativistic effective potential

$$\gamma_e V_c - V_c^2/2m_e c^2$$

stabilizes the system at a much smaller radius at 2.84 fm.

The quadratic correction term $-V_c^2/2m_e c^2$ acts as a **short-range attractive contribution**, allowing the virial balance condition to be satisfied even when the electron is highly relativistic.

Figure 5 shows that two distinct radii fulfill the virial equilibrium: one at the Bohr-scale (normal hydrogen) and a second, much smaller solution at $r \sim 2.84$ fm, corresponding to the **small-hydrogen** state.

Table 2 lists the corresponding quantities. The total binding energy remains **negative** (~ -259 keV), confirming that the configuration represents a true bound state. The entries with $n = 2$ reflect different de Broglie numbers and are included to show the robustness of the virial solution; we focus on $n = 1$ as the ground configuration.

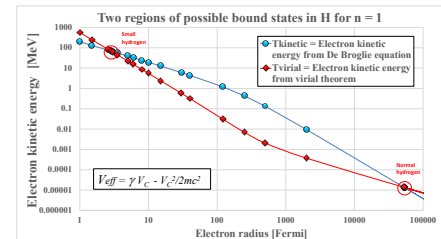


Figure 5 Virial-theorem solutions showing two stability regions—one for normal hydrogen and one for small hydrogen—calculated for $V_{\text{eff}} = \gamma V_C - V_C^2/2mc^2$.

Table 2 – Small hydrogen for $V_{\text{eff}} = \gamma V_C - V_C^2/2mc^2$

n	r_{stable} [Fermi]	$U = \gamma V_C - V_C^2/2mc^2$ [MeV]	T_{kinetic} [MeV]	$M(\text{pe}^-)^*$ [MeV/c ²]	E_{BE}^{**} [keV]
1	2.8386	-69.275	69.016	938.524	-259.3
2	2.8283	-139.371	139.115	938.527	-255.7

* Mass of small hydrogen: $M(\text{pe}^-) = m_{\text{proton}} + \gamma m_{\text{electron}} - |U|$

** Binding energy: $E_{\text{BE}} = T_{\text{kinetic energy}} - |U|$.

As a cross-check, we used Lucha's virial stability condition. Figure 6 confirms that stability occurs at $r \sim 2.8386$ Fermi.

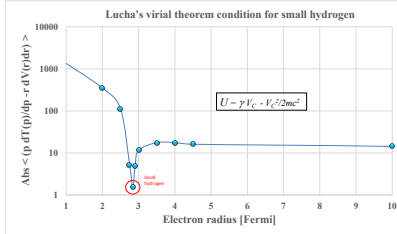


Figure 6 Numerical verification of Lucha's relativistic-virial stability condition [17], showing that the equilibrium occurs at $r \sim 2.8386$ fm.

4.3 Combined potential $U = V_{\text{eff}} + V_{(\text{Spin.B-dipole})} + V_{\text{SO}}$

We now apply the virial-stability analysis using the full effective potential $U = V_{\text{eff}} + V_{(\text{Spin.B-dipole})} + V_{\text{SO}}$.

Figure 7 compares $T_{\text{kinetic}}(r)$ and $T_{\text{virial}}(r)$ evaluated from Eqs. (10–12). Two distinct radii satisfy the virial equilibrium condition $T_{\text{kinetic}}(r) = T_{\text{virial}}(r)$, corresponding to:

1. the ordinary hydrogen ground state, and
2. a tightly bound configuration at **femtometer scale**.

Thus, the inclusion of the spin–magnetic term preserves the existence of a compact small-hydrogen solution.

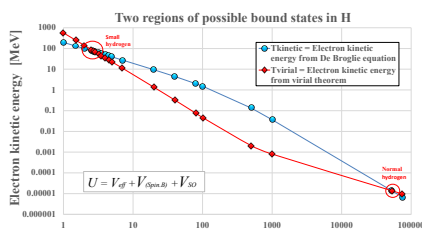


Figure 7 Comparison of T_{kinetic} and T_{virial} using the full potential $V_{\text{eff}} + V_{(\text{Spin.B-dipole})} + V_{\text{SO}}$. Two regions of stability appear: one corresponding to normal hydrogen and one at small radius.

To check internal consistency, we apply the **relativistic virial condition** (Method B, Eq. (15)). Figure 8 shows the solution of

$$((\mathbf{p}\mathbf{c})^2/\sqrt{((\mathbf{p}\mathbf{c})^2 + (m_e c^2)^2)} - \mathbf{r} \partial/\partial \mathbf{r} (U) = 0,$$

which exhibits a sharp minimum at $r \sim 2.84515$ fm. The width of this minimum is extremely narrow: FWHM ~ 0.5 fm, indicating a very tightly localized bound state.

Table 3 quantify various variables related to this solution.

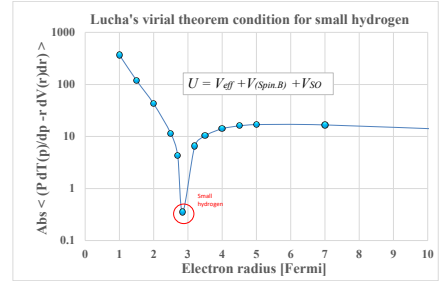


Figure 8 Solution of the relativistic virial equation (Method B). A sharp dip at $r \sim 2.8451$ fm confirms a stable compact solution.

Table 3 Small hydrogen solution using potential: $U = V_{\text{eff}} + V_{(\text{Spin.B-dipole})} + V_{\text{SO}}$:

Quantity	Value
r_{stable} [fm]	2.84515
$U(r)$ [MeV]	-69.007
T_{kinetic} [MeV]	68.855
T_{virial} [MeV]	68.855
B_{dipole} [T]	1.225×10^{11}
$V_{(\text{spin.B})}$ [MeV]	-0.05223
V_{eff} [MeV]	-68.955
V_{SO} [MeV]	$+4.06 \times 10^{-7}$ for $\ell=1, s=1/2$ -8.15×10^{-7} for $\ell=1, s=-1/2$ 0 for $\ell=0$
E_{BE} [keV]	-152.1
Mass [MeV/c ²]	938.63

The inclusion of the spin–magnetic term does not change the central binding energy predicted by the effective potential V_{eff} , which yields a spin-averaged value of $E_{\text{central-bind}} \approx -256$ keV. However, the spin-magnetic interaction **splits** this level into two hyperfine states separated by $\Delta E_{\text{hf}} \approx 100$ keV, consistent with the estimate

$$\Delta E_{\text{hf}} = 2 |V_{(\text{Spin.B})}| \sim 2 \times 52 \text{ keV} \sim 104 \text{ keV}.$$

The two resulting hyperfine energies are therefore, $E_{\uparrow\downarrow} \sim -0.152$ MeV and $E_{\uparrow\uparrow} \sim -0.360$ MeV, which bracket the central value symmetrically about ≈ -0.256 MeV.

Thus the **physical binding energy** of the small-hydrogen ground configuration is the central value (≈ -256 keV), while the **±50–60 keV hyperfine displacement** around that value generates the experimentally observable splitting.

Interpretation

- V_{eff} provides the dominant binding and sets the central depth (~ 256 keV).
- The spin-magnetic interaction is the next-largest term (~ 52 keV for aligned vs anti-aligned spin), producing a hyperfine splitting of $\Delta E_{\text{hf}} \approx 100 \pm 30$ keV.
- The **spin-orbit term** V_{SO} is suppressed by $(1/\gamma_e)^2$ and contributes only $|V_{\text{SO}}| \sim 10^{-7}$ MeV, negligible for both binding and hyperfine structure.
- The resulting small-hydrogen mass is $M(\text{pe}^-) = m_p + \gamma_e m_e - |E_{\text{central bind}}| \sim 938.63$ MeV/c², which lies approximately 0.93 MeV/c² below the neutron mass.
- Earlier models (e.g., early DDL-based work) predicted a ~ 0.509 MeV binding, suggesting a possible link to the Galactic 511 keV line. With the corrected relativistic virial analysis, including - finite-

size, spin-magnetic, and spin-orbit terms – the predicted binding is lower (~152–360 keV) and thus does not explain the 511 keV Galactic line.

Table 4 summarizes typical parameters of small and normal hydrogen.

Table 4 – Small hydrogen properties:

Variable	Normal hydrogen	Small hydrogen
n	1	1
Electron radius	0.529 Å	2.845 Fermi
Electron de Broglie wavelength	3.322 Å	17.88 Fermi
Electron de Broglie wave frequency	$\sim 6.6 \times 10^{15}$ Hz	$\sim 1.68 \times 10^{22}$ Hz
Electron $\beta = v/c$	$\sim 7.3 \times 10^{-3}$	~ 0.9999729
Electron γ_e	1.0000266	135.746
Total mass $M(p_e)$	938.78 MeV/c ²	938.63 MeV/c ²

Thus, the small-hydrogen mass is *slightly below* the neutron mass, and significantly below $m_p + m_e$, making the state stable under perturbations.

Light nuclei (e.g., He, Be, C) may also support analogous tight-bound states if the incident electron energy is sufficiently tuned. Such atoms would chemically mimic nuclei with effective charge (Z-1).

5. Heisenberg uncertainty principle

The spatial confinement of the electron in a small hydrogen state ($\Delta x \lesssim 2\text{--}3$ fm) implies a momentum uncertainty $\Delta p \gtrsim \hbar/(2\Delta x) \approx 100\text{--}200$ MeV/c. Such momenta correspond to electron Lorentz factors $\gamma_e \approx 100\text{--}200$, consistent with the relativistic regime assumed in the virial analysis. The corresponding kinetic energy increase is balanced by the strong short-range effective potential V_{eff} , which becomes much larger than the Coulomb potential at femtometer scales. A complete assessment of this relativistic stabilization requires a full QFT treatment of the two-body bound state; however, the uncertainty principle does not preclude the existence of such a tightly bound state. Rather, it *motivates* the requirement of a relativistic binding mechanism.

6. Interactions of small hydrogen

Because small hydrogen is electrically neutral and extremely compact ($r \approx 3$ fm), its electromagnetic scattering cross-section in matter is expected to be very small. At astrophysically relevant velocities, its kinetic energy per atom is typically only tens to hundreds of keV (e.g., ~ 105 keV at 4500 km/s), insufficient to ionize the bound electron or cause nuclear disruption. Thus, small hydrogen would deposit negligible dE/dx in gas or solids and interact primarily via gravity.

At thermal energies, however, the absence of a large Coulomb barrier may allow small hydrogen to be captured by positively charged nuclei. The cross-section for such capture is not presently known and likely depends on short-range QED and nuclear structure. At collision energies comparable to or exceeding the binding energy, the atom may be ionized; at GeV-scale energies, it would behave similarly to a neutron in initiating hadronic cascades.

7. Can small hydrogen atoms be detected ?

Formation of small hydrogen requires that the proton and electron have matched velocities and the electron possess a femtometer-scale de Broglie wavelength; such conditions occur only in extremely energetic environments (e.g., early Universe, accretion disks, relativistic plasmas).

If small hydrogen exists today, laboratory detection would rely on *its interactions with nuclei*. Its small size allows it to penetrate atomic electron clouds and approach nuclei with reduced Coulomb repulsion. For certain targets—such as boron—the capture of a small hydrogen atom could destabilize the nucleus and lead to characteristic emission products (e.g., α -emission), providing an experimental signature.

Additionally, atoms containing a bound small-hydrogen state would have electronic structures resembling atoms of charge Z-1, offering a possible spectroscopic search strategy.

8. Astrophysics implications

If small hydrogen exists today, its most direct electromagnetic signatures would be

- (a) a hyperfine transition near 100 ± 30 keV, and
- (b) two binding-energy lines near ~ 152 and ~ 360 keV, (the spin-averaged binding ~ 256 keV)

The $\approx 100\text{--}200$ keV band has not been systematically searched with high-sensitivity instrumentation. A dedicated observational search in this window, with energy resolution at the few-keV level and good control of instrumental backgrounds, would directly test the small-hydrogen hyperfine prediction.

8.1 Galactic Rotation Curves and Cosmic Time Evolution

If small hydrogen is produced predominantly in energetic stellar environments (e.g., core-collapse supernovae, AGN jets, black holes, or strong-shock regions), its abundance would naturally **grow with cosmic time** as more stars form and die. In that case, one might qualitatively expect older galaxies to show a larger contribution from small hydrogen to their dynamical mass budget. **This scenario does not require the absence of other dark-matter particles.**

Genzel et al. [21] have shown that massive star-forming galaxies at redshifts $z \sim 0.6\text{--}2.6$ (panel a) appear largely **baryon-dominated**, with rotation velocities that decline at large radii. By contrast, present-day galaxies at $z \sim 0$ (panel b), such as the Milky Way or M31, show extended, nearly flat rotation curves that are conventionally attributed to dark matter halos. In the context of this model, this evolution is *consistent with* (but does not demonstrate) a scenario in which small hydrogen is gradually produced in stellar processes and accumulates over billions of years, enhancing the effective dark component in older galaxies.

This trend does not imply the *absence* of dark matter in early galaxies, nor does it uniquely favor small hydrogen. Rather, it suggests that at least part of the dark component may be **acquired or enhanced over time**, which is

compatible with a late-production scenario for small hydrogen.

Additional support for such a possibility comes from galaxies like NGC 1277, where dynamical modeling indicates little or no dark matter within the optical radius [22]. This shows that not all massive galaxies must possess a substantial inner dark halo at all epochs. In a small-hydrogen framework, one could interpret such systems as environments where little late-time production or retention of small hydrogen has occurred. This is **consistent with**, though not evidence for, scenarios in which small-hydrogen contributes to the dark mass in some galaxies but not others, depending on their formation and feedback histories.

If small hydrogen existed in the early Universe, its cosmological abundance would be constrained by Big Bang Nucleosynthesis (BBN), which tolerates at most of order $\sim 1\%$ deviation from observed light-element abundances [23]. A quantitative model of small-hydrogen production during or after BBN is beyond the scope of the present work; we simply note that any viable early-Universe scenario must satisfy this bound.

8.3 Cluster Collisions (Bullet Cluster)

The Bullet Cluster provides a well-known testbed for dark-matter candidates [24,25]. In the small-hydrogen picture, the Bullet Cluster's dark component would be composed primarily of neutral, compact $p-e^-$ atoms with mass $\sim 938.6 \text{ MeV}/c^2$.

For a relative collision velocity of $\sim 1310 \text{ km/s}$, the kinetic energy of a single small-hydrogen atom is of order $\sim 10 \text{ keV}$, well below the $\sim 152 \text{ keV}$ binding energy inferred from the virial analysis. As a result, cluster-scale collisions would not ionize small hydrogen efficiently; the atoms would remain intact and interact only weakly with the intracluster plasma, while still contributing to gravitational lensing. In this sense, small hydrogen could reproduce the **collisionless behavior** required to explain the observed offset between the X-ray gas and the lensing mass in the Bullet Cluster. A dedicated simulation would be required to test this quantitatively.

8.4 Possible connection to INTEGRAL MeV lines

Several MeV-scale γ -ray lines observed by INTEGRAL/SPI are conventionally attributed to thermal-neutron capture in the spacecraft and detector materials. However, the INTEGRAL team notes that the richness and relative strength of these lines are difficult to reproduce with existing Monte-Carlo simulations, and that the underlying activation and capture processes are not yet fully understood [26]. This does not imply any problem with the measurements; rather, it reflects the inherent complexity of background production in low-mass, high-altitude instruments.¹

This modeling uncertainty motivates the value of a future mission with minimal surrounding mass, low-activation

materials, and an orbit far from the Earth-Sun system. Such an instrument would significantly reduce neutron-capture backgrounds and enable a cleaner search for narrow MeV-scale features of any origin, including the **$\sim 70\text{--}360 \text{ keV transitions predicted by the small-hydrogen model}$** .

Conclusion

Using a relativistic virial-theorem approach, we identify a self-consistent and stable compact electron-proton configuration at femtometer scales. The model predicts a bound state with a central (spin-averaged) binding energy of $\sim 256 \text{ keV}$, split into two hyperfine levels at $\sim 152 \text{ keV}$ and $\sim 360 \text{ keV}$, corresponding to a **hyperfine separation** of $\sim 100 \pm 30 \text{ keV}$. These values define direct and experimentally testable signatures. The virial method used here avoids the limitations of single-particle Dirac treatments while capturing the dominant relativistic and finite-size effects required at these radii.

Although a full two-body Quantum Field Theory calculation including the proton's internal QCD structure is ultimately necessary for a complete description, the present analysis provides a physically coherent argument for the possible existence of such states. The next essential step is a program of targeted laboratory and space-based searches capable of probing the **$\sim 100 \text{ keV region with sufficient sensitivity}$** , and with coverage extending across the broader **$\sim 70\text{--}360 \text{ keV band}$** indicated by the virial analysis.

The purpose of this paper is to motivate and guide these experimental investigations. Appendix #2 discusses concrete proposals how to detect it.

ACKNOWLEDGEMENTS

I would like to thank late J. Bjorken for not considering the idea of small hydrogen as crazy, and recommending to discuss it with S. Brodsky. I thank S. Brodsky for providing critical comments. I also thank J. Vary for discussing some details of his QED model. I thank R. Waggoner for discussion about details of the BBN model.

APPENDIX #1

Relation to Lagrangian, Hamiltonian, and Virial Formulations

The virial-equilibrium method used in this paper is not ad hoc: it follows directly from the general variational structure of classical, relativistic, and quantum dynamics. Here we summarize how the relativistic virial condition

¹ The INTEGRAL/SPI team themselves note the difficulty of modeling the MeV background [26]: "Thermal neutron capture is responsible for numerous and strong lines at several MeV; their unexpected presence

poses a difficult challenge for our physical understanding of instrumental backgrounds and for Monte Carlo codes."

arises from the Lagrangian and Hamiltonian formalisms and how quantum mechanics restricts the allowed radii.

1. Relativistic Lagrangian for a particle in a central potential

For an electron moving in a spherically symmetric potential $U(r)$, the relativistic **Lagrangian** is

$$L(r) = -mc^2\gamma_e - U(r)$$

with $\gamma_e = 1/\sqrt{1 - (v/c)^2}$.

The **action** is

$$S = \int (T(r) - U(r))dt$$

and the physical path is selected by the **stationary-action** condition:

$$\delta S = 0$$

This principle is universal: it underlies classical mechanics, optics (Fermat's principle), general relativity, electrodynamics, and quantum field theory (via the path integral).

2. Stationary action → Virial relation for periodic orbits

For periodic motion in a central potential, applying $\delta S = 0$ and averaging over one orbit yields the relativistic virial theorem:

$$\langle \mathbf{p} \cdot \mathbf{v} \rangle = \langle r \frac{dU}{dr} \rangle.$$

For circular (or time-averaged) relativistic motion this becomes:

$$T_{\text{kinetic}}(r_{\text{stable}}) = T_{\text{virial}}(r_{\text{stable}})$$

Which is exactly the **Method A** used in the main text.

Thus, the virial method corresponds to applying the stationary-action principle at the radius where the orbit becomes extremal.

3. Hamiltonian Formulation

The canonical momentum obtained from the Lagrangian is

$$\mathbf{p} = \frac{\partial L}{\partial v} = m\gamma_e \mathbf{v}$$

The corresponding Hamiltonian is

$$H = \mathbf{p} \cdot \mathbf{v} - L = \gamma_e mc^2 + U(r)$$

which is simply the total relativistic total energy.

Hamilton's equations, $dr/dt = \partial H/\partial p$, $dp_r/dt = \partial H/\partial r$ yield, for circular orbits, the equilibrium condition

$$\frac{\partial H}{\partial r} \bigg|_{r=r_{\text{stable}}} = 0.$$

Evaluating this gives

$$\frac{p^2 c^2}{\sqrt{p^2 c^2 + m^2 c^4}} = r \frac{dU}{dr},$$

which is *identical* to the virial equilibrium equation (**Method B**) used in the main text. Thus:

Hamiltonian stationarity \leftrightarrow **stationary action** \leftrightarrow **virial equilibrium**.

This validates the virial solution as the radius that extremizes the Hamiltonian (or action) for relativistic motion in a central field.

4. Role of Quantum Mechanics

The stationary-action solutions alone form a continuum of possible radii. Quantum mechanics restricts these through:

- **de Broglie standing-wave condition**, $\lambda = 2\pi r / n$,
- **relativistic kinetic energy**,
- **spin-dependent interactions**,
- **finite-size nuclear potentials**.

Thus, quantum conditions **select discrete radii** at which the stationary-action solutions are physically allowed—precisely the radii at which the virial equalities were evaluated in this paper. The virial method therefore represents:

classical stationary-action structure + quantum de Broglie constraint + relativistic energy balance.

APPENDIX #2

Proposed Strategies for the Experimental Detection of Small Hydrogen

Direct detection of small hydrogen

A. Formation of normal hydrogen

The capture of an electron into ordinary hydrogen provides a useful analogy.

A thermal electron approaching a thermal proton is first captured into a high-lying state, then cascades to the ground level, releasing ~ 13.6 eV. The ground-state orbital radius (0.529 Å), de Broglie wavelength (~ 3.22 Å), and kinetic energy (~ 13.6 eV) together satisfy the virial theorem. Efficient capture requires that the electron and proton energies satisfy the corresponding wavelength and binding conditions.

We apply the same considering formation of a compact e-p state.

B. Accelerator-Based Test to detect small hydrogen

Tables 3–4 of the main text characterize the compact state (“Small hydrogen”) by:

- radius $r \sim 2.84$ fm,
- de Broglie wavelength $\lambda \sim 17.9$ fm,
- electron kinetic energy $T_{\text{kinetic}} \sim 68.855$ MeV,
- electron Lorentz factor $\lambda \sim 135.746$ fm and $\beta = 0.9999729$.

Efficient formation requires the proton to have the **same velocity** as the electron. For $\beta = 0.9999729$, the corresponding proton total energy is: $E_{\text{Proton}} \sim 127.37$ GeV.

Thus, the experimental configuration requires co-propagating relativistic electron and proton beams, as sketched in Fig. 8a. In the rest frame of the co-moving e-p pair, formation of the compact state would emit a photon with: $E_{\text{Source}} \approx 150$ keV.

Doppler-boosted gamma signal

In the laboratory frame, the photon energy is:

$$E_{\text{Observed}} = E_{\text{Source}} / [\gamma (1 - \beta \cos \phi)] \quad (14)$$

where ϕ is the angle between the photon direction and the beam axis (Fig. 8b).

- At $\phi \sim 6.95^\circ$, $E_{\text{Observed}} \sim E_{\text{Source}}$.
- At $\phi = 0^\circ$, $E_{\text{Observed}} \sim 40.77$ MeV, a value extremely sensitive to small uncertainties in γ , and therefore unsuitable for a precision line search.

Therefore, the optimal detection region is **5–20°**, where the Doppler-boosted line remains near the intrinsic ~ 100 –150 keV scale.

Experimental Configuration

If a compact e-p state is formed, it would subsequently interact in a calorimeter, dissociating into:

- one electromagnetic shower (electron),
- one hadronic shower (proton),

nearly collinear because of the large Lorentz boost. Their combined energy would recover the small-hydrogen mass: ~ 938.63 MeV/c².

Suitable facilities include **BNL**, **Fermilab**, and **CERN**. The CERN SPS already provides protons near 127 GeV; an accompanying 68–70 MeV electron beamline would be sufficient.

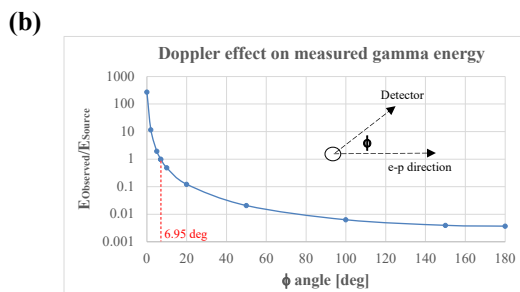
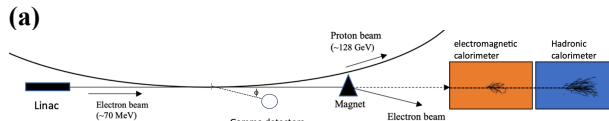


Figure 8 (a) Schematic concept to prove that the small hydrogen exists. Proton beam is brought tangentially to electron beam so that both beams travel parallel to each other for some distance. If the small hydrogen is formed, it will emit a 150 keV gamma in the two-particle rest frame, while electrons are deflected by a magnet. (b) Gamma energy is boosted by the Doppler effect to high values at very forward direction from a source traveling at velocities close to velocity of light – see equation (14).

C. Search in High-Energy Collisions

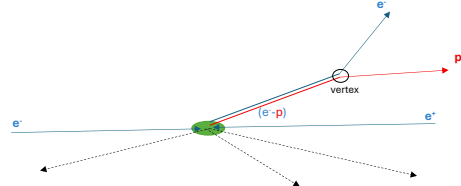
Large collider experiments (BaBar, Belle II, LHCb, CMS, ATLAS, or the EIC) could search for a compact e-p bound state produced in high-energy interactions. Depending on lifetime and decay mode, the expected signatures include:

1. **Missing-mass peak** near ~ 938.63 MeV/c², if the state is stable.

2. **No displaced vertex**, if the lifetime is very short.
3. **V-shaped decay topology** (Fig. 9a), if the lifetime is measurable.
4. **Two nearly collinear calorimeter showers** in the calorimeter (Fig. 9b), one electromagnetic and one hadronic.

These signatures are experimentally accessible.

(a)



(b)

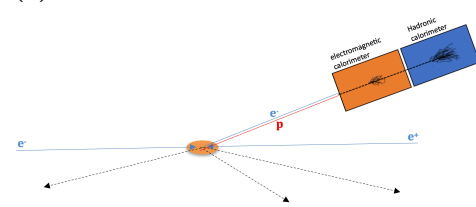


Figure 9 (a) Assuming that small hydrogen system is unstable and one can measure vertex. It will show up as a peak in the e-p effective mass distribution close to mass of the small hydrogen of ~ 938.63 MeV/c². (b) If small hydrogen is stable, it will not produce a visible track, but it would produce two collinear showers, one electron shower followed by hadronic shower of proton.

4. Satellites-based Search

A dedicated low-activation space instrument could perform a decisive test. Key capabilities include:

- sensitivity to a 100 ± 30 keV hyperfine lines,
- sensitivity to a 150 keV binding-energy line,
- **minimal nuclear-activation backgrounds**,
- **directional capability**,
- ability to distinguish **astrophysical variability** from instrumental effects.

Experience from INTEGRAL/SPI shows that activation lines are difficult to model precisely. A purpose-built low-mass detector, placed far from the Earth-Sun system, would greatly reduce backgrounds and allow a clean search for the predicted narrow features.

REFERENCES

- [1] R. Reeves, “A force of Nature”, page 114, Atlas books, New York - London, 2008.
- [2] A. Pais, “Inward bound”, page 401, Clarendon press – Oxford, 1986.
- [3] L. I. Schiff, “Quantum Mechanics”, (equation 53.16, page 470), 3rd ed., McGraw-Hill Publishing Company, New York (1968).
- [4] J. Maly and J. Va'vra, “Electron Transitions on Deep Dirac Levels I”, Fusion Technology, Vol. 24, November 1993.
- [5] J. Maly and J. Va'vra, “Electron Transitions on Deep Dirac Levels II”, Fusion Technology, Vol. 27, Jan. 1995.

[6] F.C. Smith and W.R. Johnson, "Relativistic Self-Consistent Fields with Exchange", *Phys. Rev.* 160, 136–142 (1967).

[7] B.W. Bush, J.R. Nix, *Ann. of Phys.*, 227, 97 (1993).

[8] E.E. Salpeter and H. Bethe, "A Relativistic Equation for Bound-State Problems", *Physical Review*, Vol.84, No.6, 1951.

[9] J.R. Spence and J.P. Vary, "Electron-proton resonances at low energy from a relativistic two-body wave equation", *Physics Letters B* 271 (1991) 27-31.

[10] S. J. Brodsky, H.-C. Pauli, S. S. Pinsky, "Quantum Chromodynamics and Other Field Theories on the Light Cone," *Phys. Rep.* 301, 299–486 (1998).

[11] A. Sommerfeld, "Zur Quantentheorie der Spektrallinien," *Annalen der Physik* 51, 1 (1916).

[12] P.A.M. Dirac, "The Quantum Theory of the Electron," *Proc. R. Soc. A* 117, 610 (1928).

[13] S. Flügge, "Practical Quantum Mechanics", Springer-Verlag, Berlin, 2-nd printing, 1994.

[14] S. V. Adamenko and V. I. Vysotskii, "Mechanism of synthesis of superheavy nuclei via the process of controlled electron-nuclear collapse," *Foundations of Physics Letters*, Vol. 17, No. 3, June 2004.

[15] J.L. Paillet and A. Meulenberg, "Advance on Electron Deep Orbitals of the Hydrogen Atom", *J. Condensed Matter Nucl. Sci.*, p.50, 24 (2017) 258–277.

[16] J. Gaite, ArXiv:1306.0722v1 [hep-th] 4 Jun 2013

[17] W. Lucha, *Mod. Physics Lett.*, Vol.5, No.30 (1990) 2473.

[18] https://en.wikipedia.org/wiki/Virial_theorem.

[19] D.S. Hwang et al., "Average kinetic energy of heavy quark and virial theorem", *Physics Letters B*, 406(1997)117.

[20] M. Ackermann et al., "The spectrum of isotropic diffuse gamma-ray emission between 100 MeV and 820 GeV", arXiv:1410.3696v1 [astro-ph.HE], 14 Oct 2014.

[21] R. Genzel et al., *Nature*, 543, 397–401 (16 March 2017), DOI: 10.1038/nature21685.

[22] S. Comerón et al., "The massive relic galaxy NGC 1277 is dark matter deficient", *A&A* 675 (2023).

[23] R. Wagoner, private communication, 2024, and *Ap.J.* 179, 343 (1973).

[24] Markevitch et al. "Direct Constraints on the Dark Matter Self-Interaction Cross-Section from the Merging Galaxy Cluster 1E 0657-56", *The Astrophysical Journal*, Vol. 606, pp. 819-824 (2004).

[25] Harvey et al. "The non-gravitational interactions of dark matter in colliding galaxy clusters", *Monthly Notices of the Royal Astronomical Society*, Vol. 443, Issue 4, pp. 3838-3854 (2014).

[26] G. Weidenspointner et al., *Astronomy and Astrophysics* 411, L113L11 (2003).